



# Uncover deeper insights into the impact of global research

Understand your place in the global engineering research landscape and make strategic decisions about the direction of your projects with a dynamic research intelligence tool based on the IET's renowned Inspec database.





## Precision analytics for research excellence

Enhanced features allow you to uncover deeper insights into the impact of global research and explore the elements most valuable to you. With Inspec Analytics, you can:

- Deepen your understanding of global scientific trends.
- Define the scope of research initiatives to maximise your impact.
- Assess your organisation's research output and impact.
- Evaluate the success of collaborative partnerships.

Learn more at [inspec-analytics.theiet.org](https://inspec-analytics.theiet.org)

# A novel adaptive cascade controller design on a buck–boost DC–DC converter with a fractional-order PID voltage controller and a self-tuning regulator adaptive current controller

Hasan Mollaei<sup>1</sup>  | Seyyed Morteza Ghamari<sup>1</sup>  | Seyyed Amirhossein Saadat<sup>1</sup>  |  
Patrick Wheeler<sup>2</sup> 

<sup>1</sup> Control and Robotic Faculty, Shahrood University, Semnan, Iran

<sup>2</sup> Department of Electrical and Electronic Engineering, Nottingham University, Nottingham, UK

## Correspondence

Hasan Mollaei, Control and Robotic Faculty, Shahrood University, Semnan, 7714534577, Iran.  
Email: [mortaza.ghamari@yahoo.com](mailto:mortaza.ghamari@yahoo.com);  
[h.mollaei@shahroodut.ac.ir](mailto:h.mollaei@shahroodut.ac.ir)

## Abstract

The design of a cascade controller is demonstrated for a buck–boost converter that is combined with two control loops consisting of inner and outer controllers. The outer loop is implemented by a fractional-order proportional-integrated-derivative (FO-PID) controller that works as a voltage controller and generates a reference current for the inner control loop. To provide faster dynamic performance for inner loop, a self-tuning regulator adaptive controller, which tries to regulate the current with the help of a novel improved exponential regressive least square identification in an online technique, is designed. Moreover, in the outer loop, to tune the gains of the FO-PID controller, a novel algorithm of antlion optimizer algorithm is used that offers many benefits in comparison with other algorithms. The system provided by the boost mode is a non-minimum phase system, which creates challenges for designing a stable controller. In addition, a single loop controller is proposed based on a PID controller tuned by a particle swarm optimization algorithm to be compared with the cascade controller. Cascade loop can present significant benefits to the controller such as better disturbance rejection. Finally, the strength of the presented cascade control scheme is verified in different performing situations by real-time experiments.

## 1 | INTRODUCTION

The development of DC–DC power converters provided numerous methods to produce electrical power for various applications. Meanwhile, the load connected to a converter acts as a consumer in need of different levels of voltage. buck–boost converter is an efficient topology able to perform in both step-down and step-up modes with minimum numbers of electrical components. It provides higher efficiency in wider voltage ranges and it presents lower operating duty cycle [1, 2]. Moreover, the weight and cost of this structure decreases considerably compared to other topologies that depict it as a proper alternative for industrial applications [3, 4]. Based on the zero of this system located in the right half plane in boost mode, an

unstable feature occurs as a non-minimum phase system making challenging conditions for designing an appropriate control method for the converter [5, 6]. Hence, the necessity of designing a flexible and well-behaved controller capable of compensating operational characteristics of the converter has been felt. Thus, a demand is created for control strategies with more complicated principles; this has caused a growth in the digital controllers for switching mode power supplies (SMPS) [7, 8].

Proportional-integrated-derivative (PID) and hysteresis controllers are the most common control strategies thanks to their simple structure, suitable efficiency, and appropriate cost. In [9–11], hysteresis and PID control schemes are used for the buck–boost converter to track and regulate the load voltage where a good performance can be seen; however, these are

-----  
This is an open access article under the terms of the [Creative Commons Attribution](https://creativecommons.org/licenses/by/4.0/) License, which permits use, distribution and reproduction in any medium, provided the original work is properly cited.

© 2021 The Authors. *IET Power Electronics* published by John Wiley & Sons Ltd on behalf of The Institution of Engineering and Technology

not robust against parametric variations and load uncertainties. Due to switching characteristics of the buck–boost converters, numerous control techniques are implanted for this topology, as follows: sliding-mode control [12], predictive control [13], and dead beat technique [14]. Providing a significant output signal with a very low level of overshoot and omitting the level of ringing are the main contributions presented by these controllers. Meanwhile, the complexity of predictive and dead beat control strategies makes them unpopular alternatives [15, 16]. In other words, sliding-mode control strategies can provide greater robustness during transients, parametric variations, and chattering problems.

In [17–19], different adaptive techniques are listed for the buck–boost converter. Yet, one can mention the fuzzy-PI adaptive control method tuned by Lyapunov stability, a back stepping adaptive method combined by the sliding-mode technique, and an adaptive scheme designed by I-I observer. These methods presented good dynamic performance; yet, they are not able to show good robustness against disturbances and the impact of noise has not been examined for these controllers. To surpass the weaknesses mentioned by the above papers, a predictive neural network adaptive control technique was illustrated in [20] depicting better responses rather than fuzzy neuro and fuzzy strategies [21, 22]. Additionally, the design of a novel robust adaptive controller is presented in [23, 24] by the help of a robust estimator. This technique tries to compensate for the negative impact of noise and disturbance in the identification block before applying it to the control block which depicts considerable results but is highly dependent on the estimator which can result in lower efficiency.

These papers use a single loop voltage controller to track the reference signal with a good robustness. In [25], it is highlighted that for the single loop control designs a good operation can be provided in the case of constant load. However, it is mentioned that the major drawback of the single loop controllers (SLC) are their weakness and poor performance when constant alterations happen in input supply voltage. Authors in [26] have presented that the single loop control shows lower stability since the current feedback is absent. Also, the single loop voltage controllers have no protection against short circuit faults; thus, they need additional circuitry. Overall, the main drawbacks result from the SLC for a DC–DC power converter are listed as follows: (1) high transients can be produced during its operation, (2) gains and dynamic behaviour of the system is effected by the input supply voltage variations, (3) a greater risk of instability is reported due to the lack of a current feedback loop, and (4) there is no inherent short circuit protection [28, 29]. Various cascade control techniques are reported for power converters in [30–36] providing better stability and performance. Besides their good results, off-line methods are used to reach the ideal control gains which can decrease the efficiency of the strategy in longer time periods; however, none of them are tested in noisy situations while this is an inevitable circumstance. To fulfill all the issues discussed in these works, an adaptive cascade controller is designed here. This work has an online self-tuning inner loop which can provide better parametric optimization in challenging conditions resulting in better outputs. In addi-

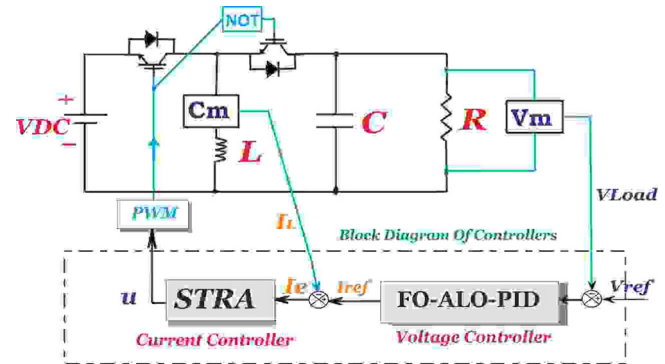


FIGURE 1 Structure of the cascade controller on buck–boost converter

tion, the outer loop utilizes an improved fractional-order PID (FO-PID) control strategy that can improve robustness of this structure.

Over the recent decade, fractional calculus perspective has been used to redesign, adapt and explore control approaches to improve dynamic response and model accuracy. In [37–39], some of the major outcomes behind utilizing fractional calculus are listed as follows:

- Robustness against parameter variations.
- Lower noise based on lower order derivatives.
- An extra degree of freedom providing better system description.
- Great system approximation with lumped parameters.
- Better adaption of system frequency behaviour.

Regarding fractional calculus, several considerable results are reported which verify the efficiency of a fractional-order term in control techniques.

To better clarify control structure on the converter, Figure 1 is plotted with two loops. First, a FO-PID compensator tries to regulate the voltage of load in the outer loop and then generates a reference current for the inner loop of the adaptive current controller to fire the switch as an inner loop.

The novelty of this paper is focused on designing an adaptive cascade controller with an outer-voltage controller of the FO-ALO-PID technique and an inner-current controller of the self-tuning regulator adaptive (STRA) strategy along with a novel improved exponential regressive least square (IERLS) identification. Contributions provided by this method are listed below:

- An adaptive cascade controller is presented with stability analysis insurance in different conditions.
- The closed-loop structure is verified with different disturbances and noise.
- The transient response and the robustness of the controller is improved in different conditions particularly parametric variations and noise robustness when the system is subject to the unwanted disturbance.
- Better PID gains are tuned by an antlion optimizer (ALO) algorithm which improved the performance of the controller.

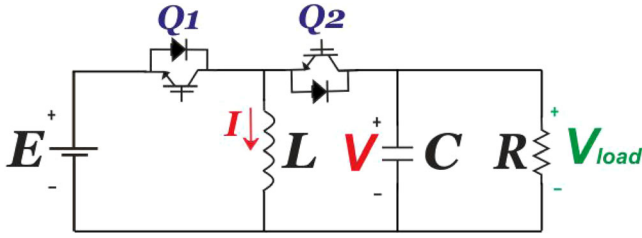


FIGURE 2 Buck-boost converter

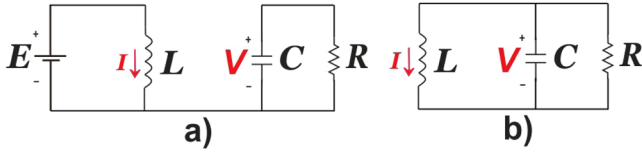


FIGURE 3 Buck-boost converter operation; (a) charging mode, (b) discharging mode

- An improved identification technique is utilized providing better parametric estimation for the adaptive controller.
- Results in both experimental and simulation environments confirm the efficiency of the proposed adaptive cascade controller.

## 2 | BUCK-BOOST CONVERTER

This topology has components as follows: voltage source ( $E$ ), two switches named  $Q_1$  and  $Q_2$ , capacitor ( $C$ ), inductor ( $L$ ), and resistor  $R$  as load. In Figure 2, a circuit schematic of this structure is plotted considering switching devices. In Figure 2, two operational modes are fired by the switching function of  $u$ . Figure 3 depicts the circuit topology based on the control variable,  $u$ ; when  $Q_1$  is switching and  $Q_2$  is off, the converter works in buck mode; whereas, when  $Q_2$  is switching and  $Q_1$  is off, the converter operates in the boost condition [47].

To drive the transfer functions of this converter, it must be mentioned that transfer functions contain a right half plane zero. Based on the location of zero in boost mode, a non-minimum phase transfer function is provided [40, 41]. The state space representations for the two modes are illustrated in Equation (1).

$$\begin{aligned} \dot{x} &= Ax + Bu, & y &= Cx \\ x &= \begin{bmatrix} I \\ V_c \end{bmatrix}; & A &= \begin{bmatrix} 0 & -\frac{1-s}{L} \\ -\frac{1-s}{C} & -\frac{1}{RC} \end{bmatrix} \\ B &= \begin{bmatrix} \frac{E*s}{L} \\ 0 \end{bmatrix}; & C &= \begin{bmatrix} 1 & 0 \\ 0 & -1 \end{bmatrix}, \end{aligned} \quad (1)$$

where  $s$  is the switching mode with corresponding values of 0 and 1. Moreover, the STR adaptive controller needs a digital discrete transfer function of the proposed system where zero-order

hold (ZOH) drives this duty.

$$G(z) = \frac{Y(z)}{U(z)} = \frac{b_0 z + b_1}{z^2 + a_1 z + a_2 z}, \quad (2)$$

where unknown parameters,  $b_0$ ,  $b_1$ ,  $a_1$ , and  $a_2$ , can be obtained by using the recursive least square (RLS) identification method on the converter.

## 3 | VOLTAGE CONTROL LOOP

### 3.1 | Basics of FO calculus

Fractional-order control strategy can be explained by differential equations. On the other hand, fractional calculus provides the integrals and derivatives at an arbitrary order. The FO-PID strategy is generally generated as a result of the conventional PID controller based on fractional calculus. The prominent benefit of FO-PID controllers is the ability to better tune the parameters for improving the design flexibility. General calculus operator is illustrated in (3).

$${}_a D_b^\alpha = \begin{cases} \frac{d^\alpha}{dt^\alpha} & R(\alpha) > 1, \\ 1 & R(\alpha) = 0, \\ \int_a^b (dt)^{-\alpha} & R(\alpha) < 0, \end{cases} \quad (3)$$

where the operator has two lower and upper limits,  $a$  and  $b$ , and  $\alpha$  is known as the order of integration or differentiation ( $\alpha \in \mathbb{R}$ ). The fractional-order differintegrals are basically infinite dimensional linear filters. Moreover, to apply the hardware implementation, band-limited realization of fractional-order controller is inevitable. Three fundamental definitions are classified for fractional calculus [42], from which the Riemann–Liouville's differintegral definition method is utilized here. This technique is the most popular one of the three techniques [43]. Equation (4) depicts this strategy.

$${}_a D_b^\alpha f(t) = \frac{1}{\Gamma(-\alpha + m)} \frac{d^m}{dt^m} \int_a^b \frac{f(\tau)}{(-\tau + t)^{\alpha - m + 1}} d\tau, \quad (4)$$

where  $\alpha$  has the integer part of  $m$ ,  $m > \alpha > m-1$ ,  $m \in \mathbb{N}$ , the applied function is  $f(t)$  and Euler's gamma function of  $x$  has a notation of  $\Gamma(\cdot)$ . To clarify the FO-PID controller, a generalized transfer function is written in the form of (5).

$$C^{FOPID}(s) = K_p + \frac{K_i}{s^\lambda} + K_d s^\mu, \quad (5)$$

however,  $K_D$ ,  $K_I$  and  $K_P$  are the corresponding derivative, integral and proportional gains of the control procedure. Based on (5), two variables,  $\mu$  and  $\lambda$ , are added to the equation for the differintegral order operator. Considering the different structure of P, PI, PD and PID controllers,  $\mu$  and  $\lambda$  variables are selected as  $((0, 0)$ ,  $(0, 1)$ ,  $(1, 0)$  or  $(1, 1)$ ),

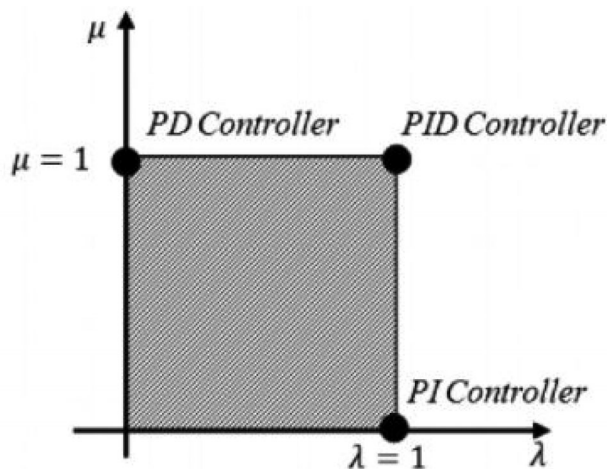


FIGURE 4 Representation of FO-PID controller

respectively. The schematic diagram of the FO-PID controller is illustrated with the  $\mu-\lambda$  plane in Figure 4 and the differentiator order is shown by it. The differentiation is defined by vertical axis while the order of the integrator may differ along horizontal axis.

### 3.2 | Optimizer algorithm of antlion

An ALO algorithm uses the process reaction between trapped ants and antlions [44]. First, ants are considered as motions in searching space and then, antlions try to catch them. Based on the fact that ants move randomly in the space, the movement of ants can be described by Equation (6).

$$X(t) = [0, c(2r(t_1) - 1), c(2r(t_2) - 1), \dots, c(2r(t_n) - 1)]. \quad (6)$$

In Equation (6), the cumulative sum is  $c$ ,  $t$  illustrates a step of random walk,  $n$  is the iteration maximum number, and  $r(t)$  is a stochastic function calculated as below:

$$r(t) = \begin{cases} 0 & \text{if } rand \leq 0.5, \\ 1 & \text{if } 0.5 < rand. \end{cases} \quad (7)$$

Next, the position of the ants is stored in the matrix of Equation (8) and will be used during the optimization.

$$M_{ANT} = \begin{bmatrix} T_{1,1} & T_{1,2} & \dots & T_{1,d} \\ T_{2,1} & T_{2,2} & \dots & T_{2,d} \\ \vdots & \vdots & \vdots & \vdots \\ T_{n,1} & T_{n,2} & \dots & T_{n,d} \end{bmatrix}, \quad (8)$$

where  $M_{ANT}$  depicts each ant's position,  $n$  is the number of ants,  $T_{i,j}$  is the amount of the  $j$ th variable (dimension) of the  $i$ th ant, and  $d$  depicts the rate of variables. To clarify the ALO algorithm better, the ants in this algorithm are as particles in the particle swarm optimization (PSO) algorithm. Moreover, an ant

position has the role of the gains for a specific solution. A fitness function is introduced in (9) to evaluate each ant during optimization:

$$M_{OA} = \begin{bmatrix} f([T_{1,1}, T_{1,2}, \dots, T_{1,d}]) \\ f([T_{2,1}, T_{2,2}, \dots, T_{2,d}]) \\ \vdots \\ f([T_{n,1}, T_{n,2}, \dots, T_{n,d}]) \end{bmatrix}, \quad (9)$$

where for saving the fitness of each ant,  $M_{OA}$  is used, the objective function is  $f$ , the number of ants is shown by  $n$ , and the amount of the  $j$ th dimension of  $i$ th ant is depicted by  $T_{i,j}$ . Furthermore, ant lions fitness values and positions must be identified and the matrices in Equation (10) can handle these duties.

$$M_{OAL} = \begin{bmatrix} f([\mathbb{I}L_{1,1}, \mathbb{I}L_{1,2}, \dots, \mathbb{I}L_{1,d}]) \\ f([\mathbb{I}L_{2,1}, \mathbb{I}L_{2,2}, \dots, \mathbb{I}L_{2,d}]) \\ \vdots \\ f([\mathbb{I}L_{n,1}, \mathbb{I}L_{n,2}, \dots, \mathbb{I}L_{n,d}]) \end{bmatrix}, \quad (10)$$

$$M_{Antlion} = \begin{bmatrix} \mathbb{I}L_{1,1} & \mathbb{I}L_{1,1} & \dots & \mathbb{I}L_{1,d} \\ \mathbb{I}L_{2,1} & \mathbb{I}L_{2,1} & \dots & \mathbb{I}L_{2,d} \\ \vdots & \vdots & \vdots & \vdots \\ \mathbb{I}L_{n,1} & \mathbb{I}L_{n,1} & \dots & \mathbb{I}L_{n,d} \end{bmatrix}.$$

In Equation (10), the storing matrix for the position of each ant lion is  $M_{Antlion}$ . Each ant's fitness stores in  $M_{OA}$ , the antlion numbers and variable, numbers are shown by  $n$  and  $d$ , and  $\mathbb{I}L_{i,j}$  depicts the  $j$ th dimension's rate of  $i$ th antlion. In every step, the position of each ant is updated by a random walk which is illustrated by (11).

$$X_i^t = \frac{(X_i^t - a_i)(b_i - c_i^t)}{d_i^t - a_i} + c_i, \quad (11)$$

where  $b_i$  illustrates maximum random walk in the  $i$ th variable,  $a_i$  can depict the minimum random walk of the  $i$ th variable,  $d_i^t$  illustrates the maximum  $i$ th variable at the  $t$ th iteration, and  $c_i^t$  shows the minimum of the  $i$ th variable at  $t$ th iteration. Alternatively, this equation must be done for every iteration to ensure random movement in the search space. In addition, ant walk is influenced by antlion traps and to have a mathematical definition of it, Equation (12) is presented. Considering (12), the updating position of ants can be driven with random walk.

$$\begin{aligned} c_i^t &= Antlion_j^t + c_i, \\ d_i^t &= Antlion_j^t + d_i, \end{aligned} \quad (12)$$

where the maximum and minimum of all variables at the  $t$ th iteration are illustrated by  $d^t$  and  $c^t$ ; however,  $d_j^t$  and  $c_j^t$  are named as the the maximum and minimum of all variables for the  $i$ th ant, and the position of the chosen  $j$ th antlion at the  $i$ th iteration is shown by  $Antlion_j^t$ .

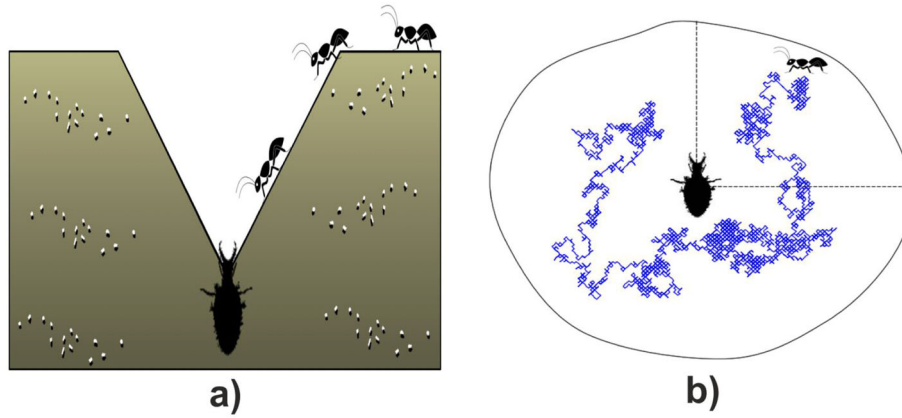


FIGURE 5 Structure of ALO algorithm: (a) antlion hunting manner, (b) roulette wheel structure inside the trap

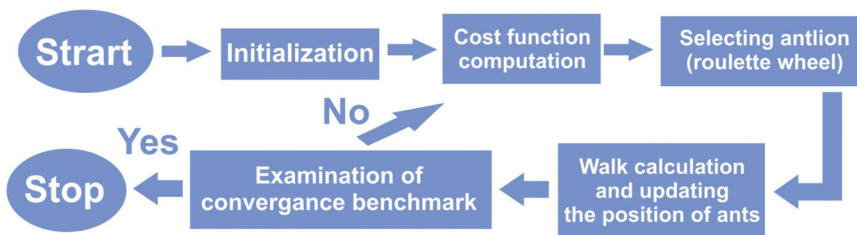


FIGURE 6 ALO algorithm flowchart

### 3.3 | Mathematical model of ALO algorithm

The antlion uses a hunting model called the roulette wheel structure [45, 46]. Here, the antlion throws sand to the edge of the pit when the ants are trapped inside it, which prevents an ant from escaping. This mechanism model can be modelled by an adaptive decrease over the radius of the ants' random walks hyper-sphere which is shown in Figure 5, while roulette wheel structure can be described by the following relations:

$$\begin{aligned} d^t &= \frac{d^t}{I}, \\ c^t &= \frac{c^t}{I}. \end{aligned} \quad (13)$$

In the above equations,  $I$  represents a fixed value that is defined as below:

$$I = 10^w \frac{t}{T}. \quad (14)$$

In the above equation, terms of  $t$ ,  $T$  and  $w$  are the current iteration, the maximum number of iterations, and an adjustable constant for exploitation of the accuracy level which is explained in (15).

$$\begin{aligned} 0.95T < t & \quad w = 6, \\ 0.9T < t & \quad w = 5, \\ 0.75T < t & \quad w = 4, \\ 0.5T < t & \quad w = 3, \\ 0.1T < t & \quad w = 2. \end{aligned} \quad (15)$$

The last step of the hunt is when the bait reaches the lowest level of the pit and the antlion can catch it. For better adaptation of this technique, one can assume that the bait is in the sand to be eaten by antlion. Therefore, the position of antlion must be adapted based on the position where the hunt has happened. This adaption is assumed to increase the chance of a new hunt which is depicted as follows:

$$Antlion_j^t = Ant_i^t; \quad \text{iff}(Ant_i^t) > f(Antlion_j^t), \quad (16)$$

where at the  $t$ th iteration, the position of the  $i$ th ant is defined by  $Ant_i^t$ . The flowchart of the ALO algorithm is demonstrated in Figure 6.

### 3.4 | Particle swarm optimization algorithm

Nowadays, optimization schemes have attracted attention based on their good performance. The PSO algorithm is a well-known optimization technique, which can be considered as an evolutionary computation technique [42]. This algorithm was reached by research on swarm. Indeed, this method of manipulating algorithms, utilizes evolutionary operators. To deal with the  $d$ -variable optimization problem, a flock of particles is applied to the  $d$ -dimensional search space. Then, random positions and velocities are selected by knowledge of their most appropriate amounts. Each particle needs a proper velocity, which can be justified related to the flying experience of itself and the other particles [43]. Figure 7 shows the calculating procedure of controllers parameters using the PSO technique.

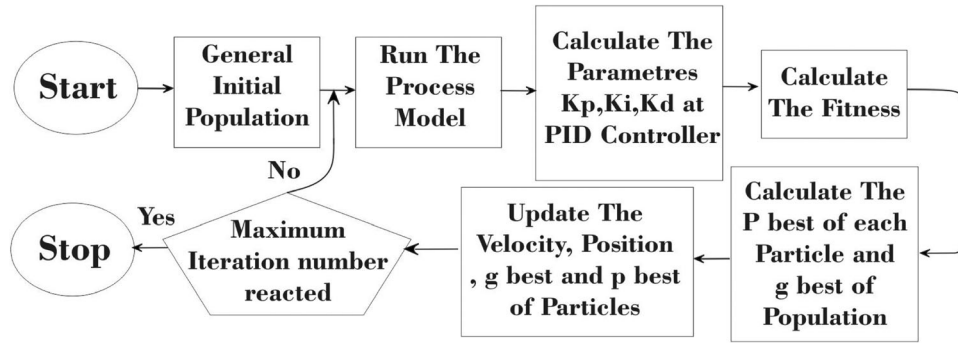


FIGURE 7 Flow chart of PSO

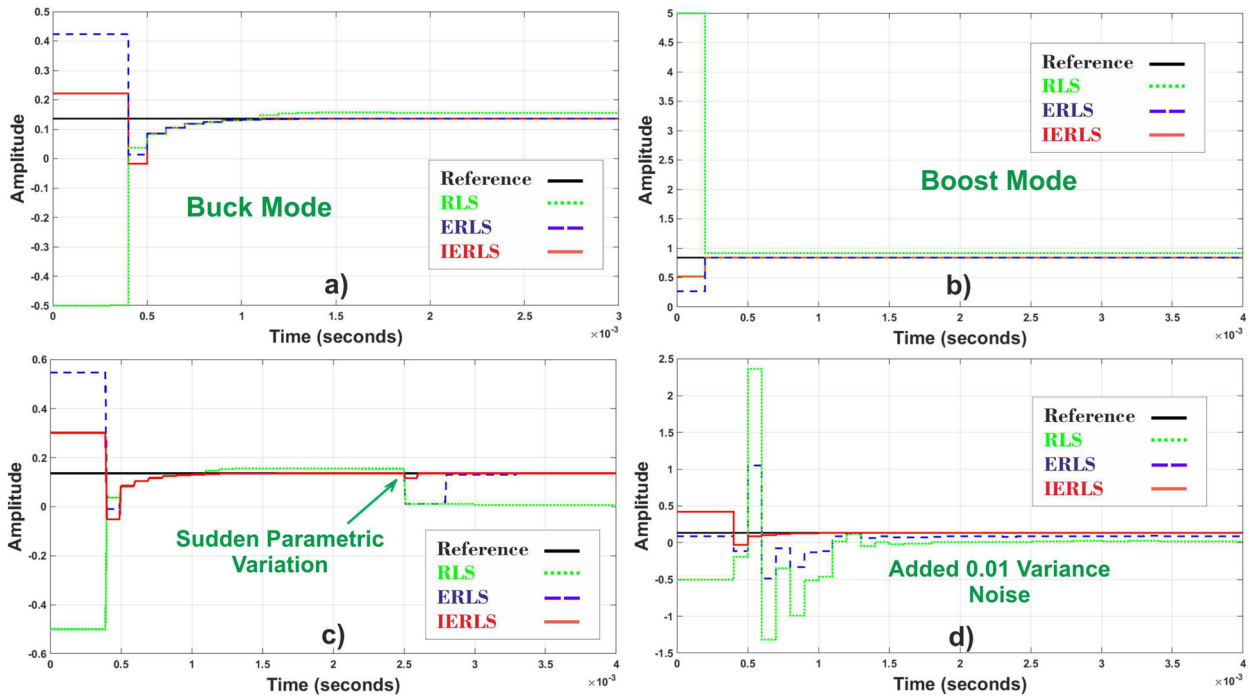


FIGURE 8 Comparison results between the proposed identification methods fed to a resistance load on the system ( $R = 10\Omega$ ): (a) convergence to the parameter of 0.1365 in buck mode, (b) convergence to the parameter of 0.83 in boost mode, (c) convergence to the parameter of 0.1365 in parametric variation, (d) convergence to the parameter of 0.1365 with injected 0.01 variance noise

## 4 | CURRENT CONTROL STRATEGY

### 4.1 | RLS identification process

RLS identification method is known as one of the most popular estimation techniques which has some benefits as follows: ease of implementation in real-time applications, low memory capacity requirement and ability of improvement for various dynamics [48, 49]. In Equation (17), the cost function of RLS technique is depicted.

$$J = \frac{1}{N} \sum_{n=1}^N e^T(k)e(k), \quad (17)$$

$$e(t) = y(k) - \hat{y}(k).$$

In Equation (17),  $e(t)$  depicts the error function; however, (18) illustrates the discrete digital transfer function.

$$y(k) = -a_2y(k-1) - a_1y(k-2) + b_1u(k-1) + b_0u(k-2). \quad (18)$$

Considering (18), one is able to write Equation (19) as follows.

$$y(k) = \phi(k)\theta(k),$$

$$\phi(k) = [u(k-1), u(k-2), -y(k-2), -y(k-1)], \quad (19)$$

$$\theta(k) = [a_2, a_1, b_1, b_0]^T.$$

Equation (19) shows two coefficients of  $\phi$  and  $\theta$  that are vectors belonging to the parameters of observation and estimation.

Meanwhile,  $u$  and  $y$  contain past values that are stored in the  $\phi$  vector. Consequently, this recursive algorithm updates the cost function regularly. Due to the fact that power converters are working in practical applications, there is a possibility of different harmful disturbances, such as parametric variation. To compensate for the impact of this damaging phenomena, a development has been made in the RLS identification algorithm. To deploy this improvement, a factor named  $\lambda$  is added to the RLS algorithm which is capable of widening the weighing function. This factor has two major advantages for the algorithm as follows: the limits of parametric estimation are enlarged causing better performance and the parametric estimation can be done considering all the current changes. Equation (20) shows this algorithm called the ‘forgetting factor algorithm’.

$$\begin{aligned}\hat{\theta}(k) &= [\theta(k-1)\phi(k)^T - y(k)]K(k) + \hat{\theta}(k-1), \\ K(k) &= (\lambda I + \phi^T(k)P(k-1)\phi(k))^{-1}\phi(k)P(k-1), \\ P(k) &= P(k-1)K(k)\phi^T(k) - P(k-1).\end{aligned}\quad (20)$$

The name of this algorithm is selected based on the additive  $\lambda$  factor named ‘time varying forgetting factor’ and is devoted as  $\lambda = e^{-\frac{b}{T_f}}$ . However,  $b$  and  $T_f$  are sampling cycle and time constant exponential forgetting, respectively. In Equation (20), two fundamental matrices are shown as  $P(k)$  and  $K(k)$  where the first matrix is the adaption matrix and the second one is the covariance matrix. It should be noted that an initial condition of  $P(0)$  is introduced for  $P(k)$  to sets the estimation process. To clarify the function of  $\lambda$  in Equation (20), the following assumption is presented: when  $\lambda$  reaches  $1 > \lambda$ ,  $K(k)$  and  $P(k)$  can reach a high rate. The prominent benefit of this structure is its continuous preparation in compensating and analysing variations that occurred in system dynamics. Equation (21) presents a trend to choose the value of  $\lambda$ .

$$\lambda(t) = \min[\lambda_0\lambda(t-1) + (1 - \lambda_0)], \quad 1 - \frac{\varepsilon^2}{\Sigma_0}, \quad (21)$$

where a limit of  $1 > \lambda > 0$  is depicted for selecting the rate of  $\lambda$  and one can consider a positive constant for  $\Sigma_0$ . Moreover, it is possible to elaborate (21) in the following stages: considering the system in steady state condition, a low rate or zero level is possible for  $\varepsilon$  where  $\lambda$  will be forced to go over 1 or stays stable at 1. Meanwhile, in the presence of disturbances, the rate of  $\varepsilon$  rises which is followed by a decrease in the value of  $\lambda$ . Consequently, it can influence the  $K(k)$  and  $P(k)$  matrices and the parametric estimation of identification procedure can be improved.

## 4.2 | Identification results of buck–boost system

Due to different disturbing phenomenon such as aging and heat of converter’s components, a small difference can be seen in Tables 1 and 2 between the estimated parameters in real-time environment and mathematical driven parameters, which

**TABLE 1** Estimation results of the buck converter model with RLS method

Model parameter	Mathematical model value	Real-time model value
$a_1$	-1.048	-1.041
$a_2$	0.136	0.125
$b_0$	1.257	1.201
$b_2$	-1.168	-1.096

**TABLE 2** Estimation results of the boost converter model with RLS method

Model parameter	Mathematical model value	Real-time model value
$a_1$	-1.048	-1.04
$a_2$	0.1365	0.1285
$b_0$	0.8378	0.797
$b_2$	-0.778	-0.597

is acceptable and cannot result in any problem in the controlling process.

To estimate the parameters of the system using an identification processor, a real-time stimulation of this converter is used considering all the components with their real values and possible derivations.

## 4.3 | Improved ERLS identification algorithm

In the RLS identification scheme, adjustment of the speed convergence in the dynamic tracking is done by  $\lambda$  as a time variable feature. In addition, whenever a small rate appears for  $\lambda$ , the convergence to parameters can be fast; however, in the presence of large disturbances, it is possible that the effect of this undesirability on the system increases consistently. Overall, the key duty of  $\lambda$  is to adapt the convergence pace with the effect of interrupting disturbances. This is named exponential RLS or ‘ERLS’ algorithm [50, 49]. Whereas,  $\lambda$  is an ideal factor that has an excellent response in actuated conditions only. To explain this circumstance, we assume that the system has not been actuated and in this situation the regressive matrix is zero which provides the following estimation relationships:

$$\begin{aligned}\frac{1}{\lambda}P(t) &= P(t+1), \\ \theta(t) &= \theta(t+1).\end{aligned}\quad (22)$$

Equation (22) illustrates that the estimation parameters of  $\theta$  with all eigenvalues of one and  $P$  matrix with all eigenvalues of  $\frac{1}{\lambda}$ , are unstable. A situation is introduced by this condition, which is known as ‘Estimator Ending’ and can be described as below: here, the estimation is fixed and if  $\lambda < 1$ , then the  $P$  matrix rises exponentially and a huge variation occurs. To solve this phenomena, conditional updating is presented, which in the



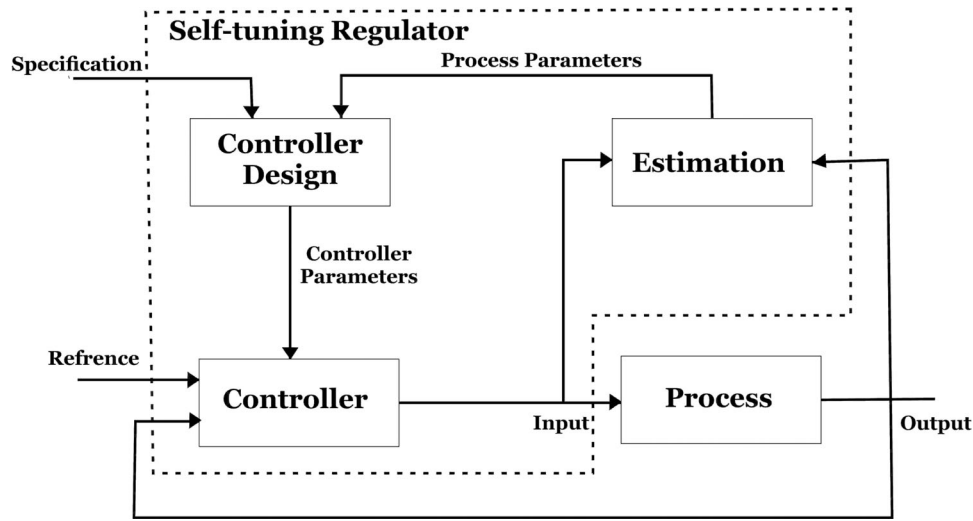


FIGURE 9 Indirect self-tuning adaptive controller block diagram

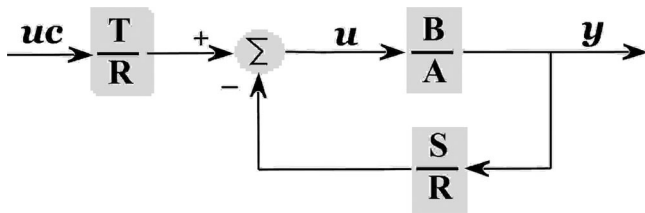


FIGURE 10 General linear controller

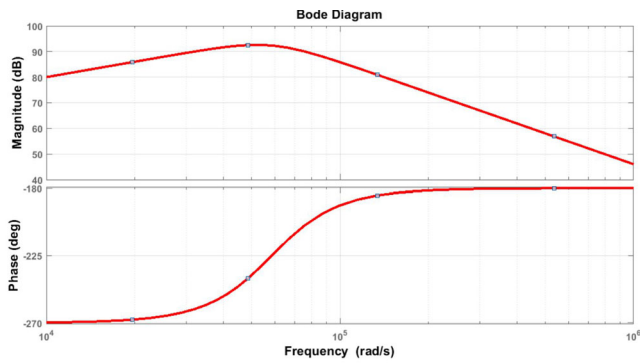


FIGURE 11 Bode plot of the current loop controller

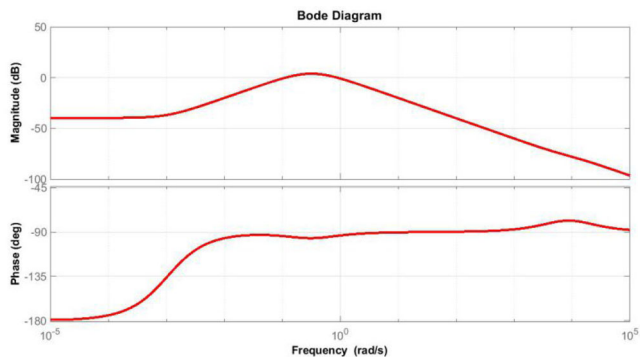


FIGURE 12 Bode plot of the voltage loop controller

estimation and covariance matrices are updated when actuation happens. As a result, the estimator is developed by a conditional updating method, which locates before the covariance matrix and updates the condition of the covariance matrix if the condition of (23) is reached and results in exponential growth avoidance.

$$\phi(t)^T P(t) \phi(t) > 2(1 - \lambda). \quad (23)$$

To ensure overcoming the estimator ending condition in the estimation performance, a new strategy of developing a covariance matrix is introduced as the ‘fixed matrix rejection method’. Additionally, for applying this strategy, the coefficients of the covariance matrix are bounded which resulted in a well-behaved performance over the ratios of the estimator. However, providing this strategy over the estimator can prevent an exponential increase of the covariance matrix when the regressive matrix is fixed. This novel improved strategy is introduced by (24).

$$\begin{aligned} \widehat{\theta}(\hat{k}) &= [y(\hat{k}) - \phi(\hat{k})^T \theta(\hat{k} - 1)] K(\hat{k}) + \widehat{\theta}(\hat{k} - 1), \\ K(\hat{k}) &= \phi(\hat{k}) P(\hat{k} - 1) [\lambda I + \phi^T(\hat{k}) \phi(\hat{k}) P(\hat{k} - 1)]^{-1}, \\ \overline{P}(\hat{k}) &= \frac{1}{\lambda} [P(\hat{k} - 1) - \frac{\phi(\hat{k}) P(\hat{k} - 1) \phi(\hat{k})^T P(\hat{k} - 1)}{I + \phi^T(\hat{k}) P(\hat{k} - 1) \phi(\hat{k})}], \\ P(\hat{k}) &= c_1 \frac{\overline{P}(\hat{k})}{r P(\hat{k})} + c_2 I. \end{aligned} \quad (24)$$

One can assume  $c_1 > 0$  and  $0 \leq c_2$ . The parameters are selected as (25):

$$\begin{aligned} \frac{c_1}{r} &\approx 10^4, \\ \phi^T \phi c_1 &\gg 1. \end{aligned} \quad (25)$$

To check the performance of different identification strategies, Figure 8 compared the performance of the presented identification methods to validate the robustness of the proposed novel algorithm.

**TABLE 3** Buck–boost converter parameter

Parameter	Value
$V_{in}$	10–40 V
$V_{out}$	5–50 V
$P_{out}$	100–180 W
$R$	10Ω
$L$	10μH
$C$	1000μF

In Figure 8 different working conditions are applied on the system to check the identification method's operation. Based on Figure 8a,b, an excellent estimation converging to the real parameter of 0.1365 in buck mode and 0.83 in boost mode for RLS, ERLS and IERLS methods are observed, yet a small difference is visible for the RLS method, which cannot cause any problem. In Figure 8c a sudden parametric variation is injected at 2.5 s, ERLS and IERLS methods show a great and fast converging, but RLS methods do not have the ability to manage this disturbance on the estimator. Next, to examine the effect of noise on the identification algorithms, a 0.01 variance noise is injected to the system in Figure 8d. In this condition, the RLS method is totally disabled and the ERLS tries to reach the estimated parameter in a long time, which can be a big difficulty for gaining the controlling signal of the cascade controller, but the IERLS method depicts a rapid parametric converging. This makes it the most appropriate alternative in challenging situations.

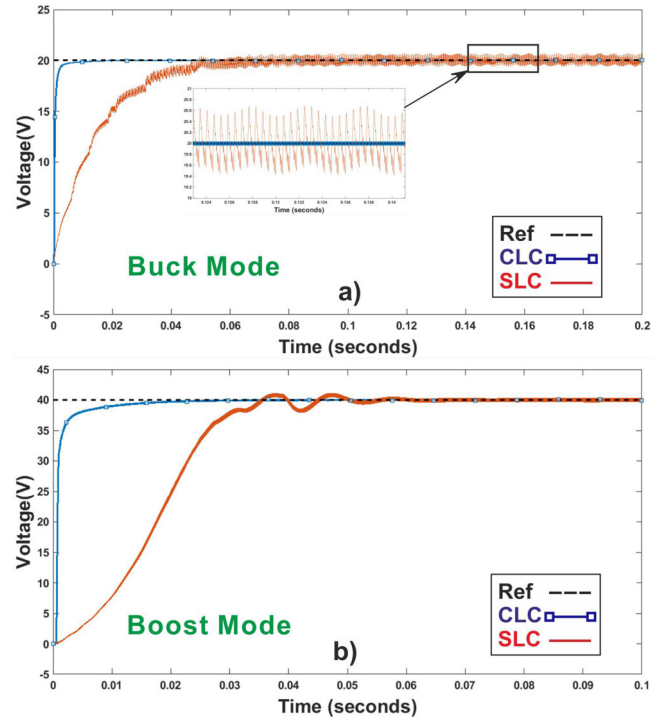
## 5 | INDIRECT SELF-TUNING REGULATOR

The chart presented in Figure 9 depicts the block diagram of a self-tuning regulator. It can be seen that the fundamental function in this diagram is based on system identification to estimate unknown parameters of the system [51]. Additionally, by reaching proper parametric estimations of the system, it is possible to offer an appropriate stability and regulation by the STR block.

The process of designing a control method is highly relevant to the closed-loop poles and zeros locations. To satisfy this issue, the pole placement method is utilized by this adaptive controller. To conclude, three stages are listed for the STR adaptive controller initializing with system transfer function identification and ending in control gains regulation by the controller based on system performance. One can assume a single input single output (SISO) system as Equation (26).

$$A(q)y(t) = B(q)(u(t) + v(t)). \quad (26)$$

In Equation (26), three variables are shown as input, output and disturbances which are shown by  $u$ ,  $y$  and  $v$  and can create the fundamental structure of the adaptive control method presented in Figure 9. One can consider the general linear form of

**FIGURE 13** Output voltage of buck–boost converter with cascade loop and single loop controllers ( $R_{load} = 10\Omega$ ): (a) tracking in buck mode, (b) tracking in boost mode**TABLE 4** Parameters of controllers

Algorithms	$K_p$	$K_I$	$K_D$	$\lambda$	$\mu$
PSO-PID	0.0327	1.49	0.58	—	—
FO-AL-PID	2.56	4.756	0.65	0.503	0.92

the adaptive controller as below:

$$Ru(t) = Tu_c(t) - S'y(t), \quad (27)$$

$w(t)$  is the desired reference for the system. However,  $T$ ,  $S$  and  $R$  are the polynomials containing the unknown parameters. Considering Figure 10, two fundamental feed backs of control law are presented for the closed-loop system; the transfer function of  $S$  depicts the negative feedback and the transfer function of  $T$  presents the feed forward. Moreover, the closed-loop

**TABLE 5** Performance comparison of the controllers

Modes	CLC			SLC		
	OS	US	$S_s$	OS	US	$S_s$
Buck	—	—	0.004 s	0.7 V	0.6 V	0.08 s
Boost	—	—	0.02 s	1.04 V	2.13 s	0.065 s

US, Undershoot; OS, overshoot;  $S_s$ , settling time.

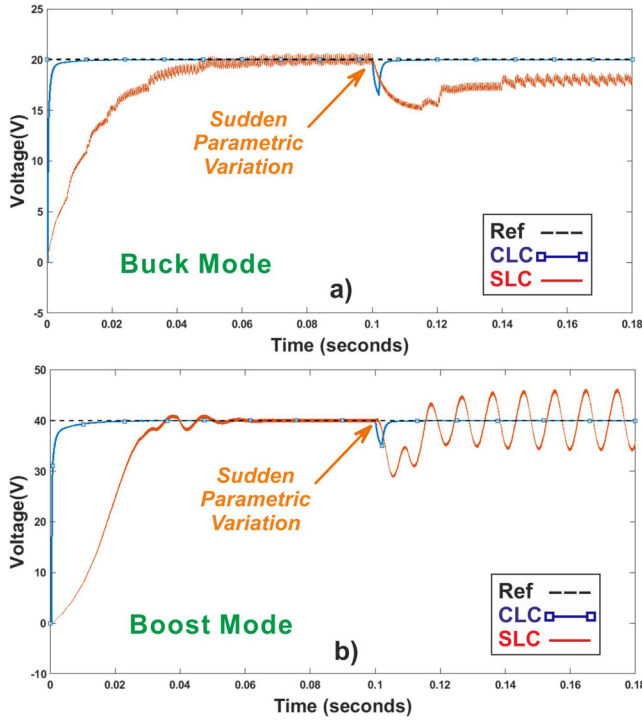


**FIGURE 14** Effect of sudden parametric variation on the controllers ( $R_{load} = 10\Omega$ ); (a) tracking in Buck mode, (b) tracking in Boost mode.

control law can be written as (28).

$$y(t) = \frac{BT}{AR + BS} u(t), \quad u(t) = \frac{AT}{AR + BS} u_c(t). \quad (28)$$

For calculating these polynomials, the ‘Diophantine equation’ is presented in (29).

$$AR + BS = A_c. \quad (29)$$

Specifying the desired closed-loop polynomial  $A_c$ , the observer polynomial, is the key idea behind the design method. By solving (30), the values of  $R$  and  $S$  can be reached; yet, the value of  $T$  and other conditions are unknown. To reach the value of  $T$ , a condition is presented below

$$\frac{BT}{AR + BS} = \frac{BT}{A_c} = \frac{B_m}{A_m}. \quad (30)$$

Here,  $A_c$  should consist of stable poles. However, one can solve the control law with Equations (30) and (29), but these equations contain many solutions. Thus, the minimum degree pole placement (MDPP) method is used with a good reliability of implementation. Additionally, two categories are classified for the STR controller named as: zero deleting indirect self-tuning regulator and zero holding indirect self-tuning regulator. The second technique is applied here to maintain the characteristics of the system.

Two transfer functions of ( $G_{(q)}^*$ ) and ( $G_{(q)}$ ) are introduced as desired and real transfer functions in (31) and (32) for describing

the proposed controller.

$$G(q) = \frac{B(q)}{A(q)} = \frac{b_0q + b_1}{q^2 + a_1q + a_2}, \quad (31)$$

$$G^*(q) = \frac{B_m}{A_m} = \frac{b_{m0}q + b_{m1}}{q^2 + a_{m1}q + a_{m2}}. \quad (32)$$

The numerator polynomial of  $B$  is presented as

$$B^+ B^-, \quad (33)$$

where  $B^-$  and  $B^+$  are the polynomials with unstable and stable zeros. The structure of the converter system is stable and is more suitable for designing a zero holding indirect self-tuning regulator method. The  $B$  polynomial can be rewritten as (34).

$$B^- = B, \quad B^+ = 1. \quad (34)$$

Considering the points mentioned, the Diophantine equation (34) is rewritten in (35).

$$AR' + B^-S = A_\sigma A_m, \quad (35)$$

$$(q^2 + a_1q + a_2)(q + r_1) + (b_0q + b_1)(s_0q + s_1) = (q^2 + a_{m1}q + a_{m2})(q + a_0). \quad (36)$$

Equation (36) helps to obtain the values of  $R$  and  $S$  but  $T$  is still unknown. Hence, two assumptions of  $BT = B_m A_0$  and  $B_m = \beta B$  are suggested for  $T$  in (28), which proposes  $T$  as (37).

$$T = \beta A_0. \quad (37)$$

Here,  $\beta = (1 + a_{m1} + a_{m2}) / (b_0 + b_1)$ .

In (38), the transfer function of a closed-loop system with adaptive controller is visible.

$$G_{cl} = \frac{y}{u_c} = \frac{BT}{AR + BS}. \quad (38)$$

## 6 | CONTROL LOOPS STABILITY

As mentioned before, the cascades controller decomposed to inner-current control and outer-voltage control loops. To verify the stability proof of the controllers, a transfer function for each loop is calculated based on the proposed system. For the inner-current loop, the closed-loop transfer function of STR method is shown in Equation (38). Based on the gains of the controller, the bode plot of inner loop is illustrated in Figure 11.

In addition, the outer loop is being analysed by its Bode plot in Figure 12. Both of the Bode plots for control loops show the stability of the cascade controller. Based on the Bode plots of

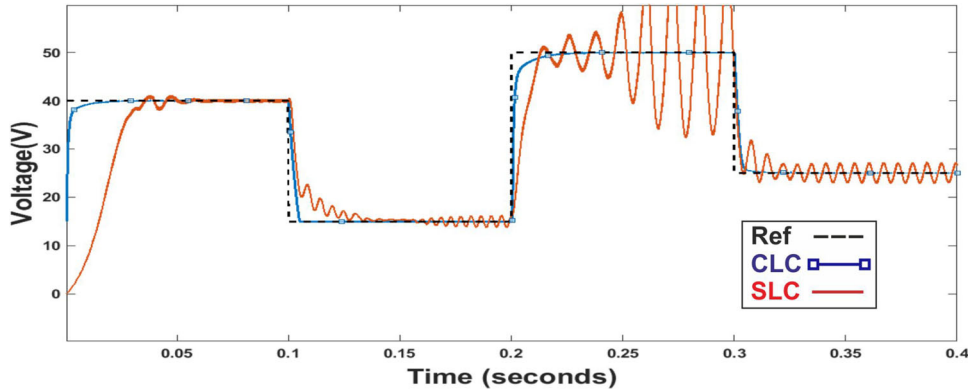


FIGURE 15 Convergence of the controllers in sudden reference voltage alterations

TABLE 6 Detailed comparison between the adaptive cascade method with the other controller in positive and negative reference voltage variations

Ref voltage changes	CLC			SLC		
	OS	US	$S_f$	OS	US	$S_f$
NS (40–15 V)	–	–	0.01 s	1.2 V	1.2 V	0.08 s
PS (15–50 V)	–	–	0.025 s	21 V	25 V	–
NS (50–25 V)	–	–	0.01 s	2.4 V	2.34 V	0.03 s

US, undershoot; OS, overshoot;  $S_f$ , settling time; NS, negative step; PS, positive step.

the both control loops and phase and gain margins, it can be seen that the stability of the controllers are proved [52].

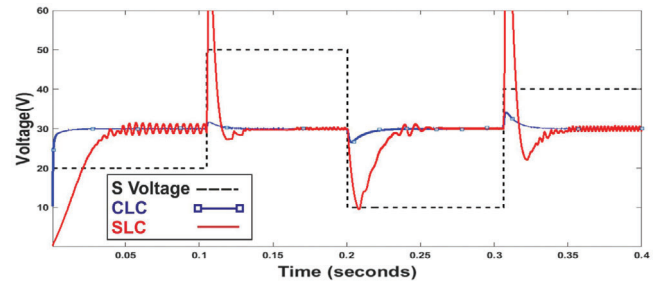


FIGURE 17 The performance of the controllers in supply voltage variations

## 7 | SIMULATION RESULTS

Here, the performance of the designed adaptive cascade controller will be tested by simulations and experiments using circuit parameters listed in Table 3. First, tracking the responses of the cascade loop controller (CLC) and PSO based PID SLC are compared in Figure 13. Moreover, the tuned gains of the PID controllers by the proposed algorithm is illustrated in Table 4. It should be noted that Matlab-simulink is used to validate the performance of the adaptive cascade method.

Figure 13 shows the controllers, converging signals to the reference signal for the buck–boost converter without applying disturbances. To better clarify the working performance of the controllers in Figure 13, a detailed comparison is carried out in Table 5. Considering the compared values of Table 5, it is clearly evident that the adaptive cascade technique illustrates better results with a faster settling time and a lower error.

As noted before, different disturbances can make some difficulties for the control process. Furthermore, to simulate the impact of parametric variation on the system, a sudden parametric change was prompted in Figure 14 for checking the performance of the controllers in compensating for this disturbance.

Based on the results provided by Figure 14 in both buck and boost modes, it is clear that adaptive cascade controller performs with a well-behaved dynamic and quicker response rather than the single loop control technique.

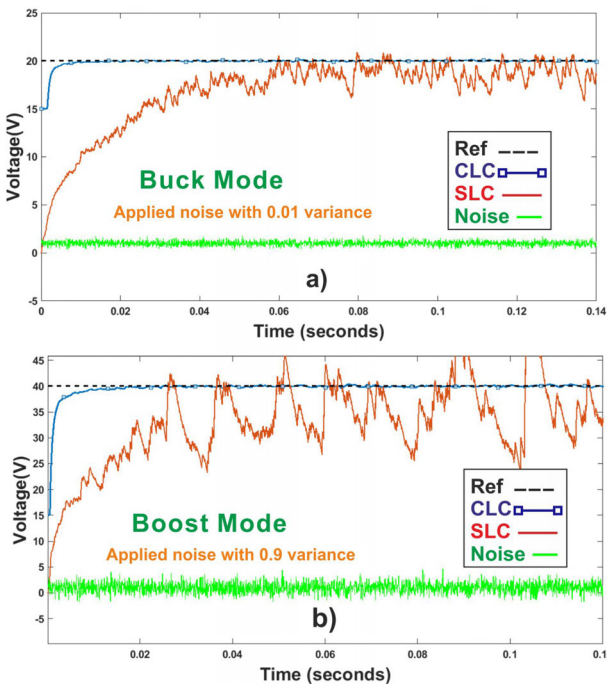
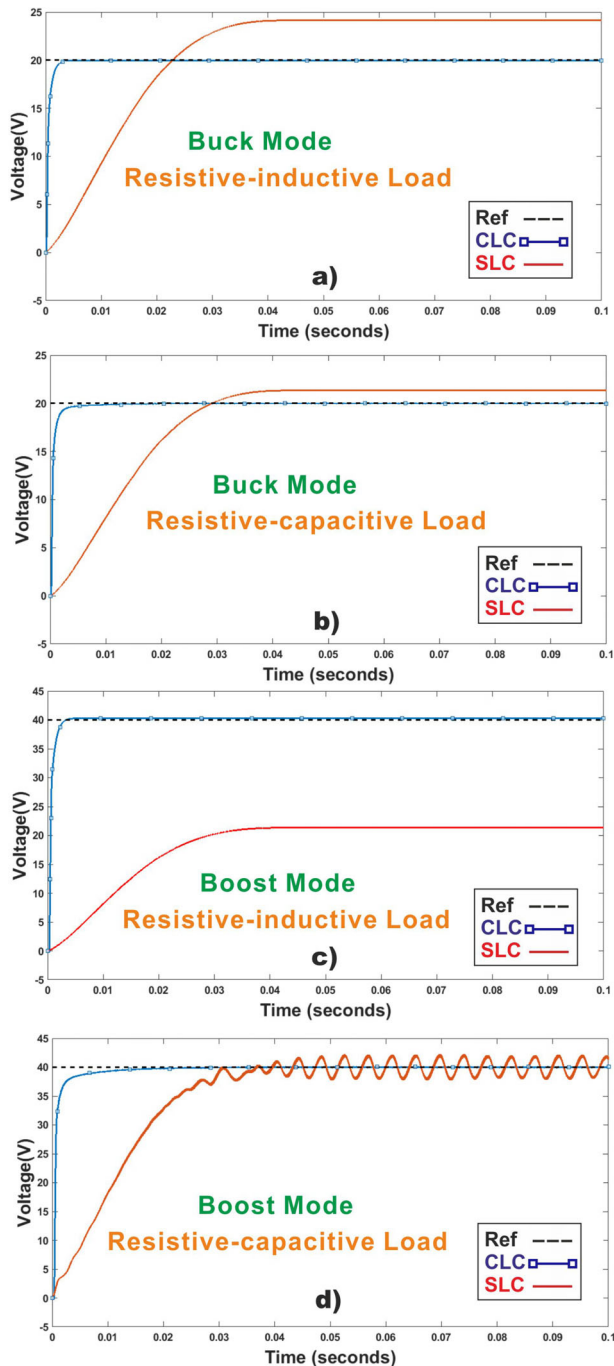
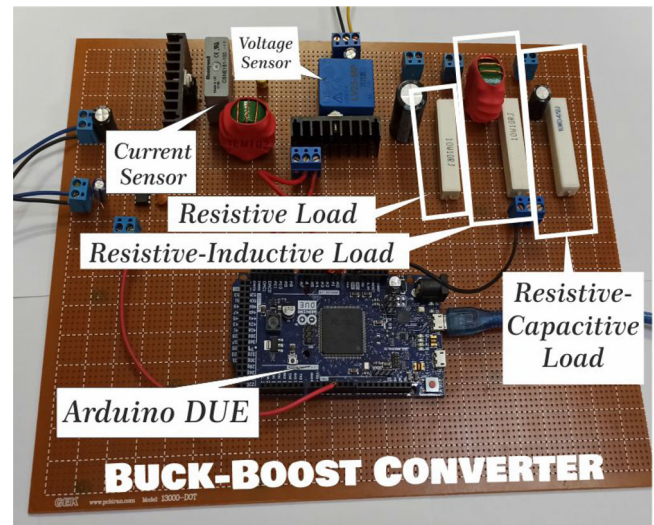


FIGURE 16 The performance of the controllers in noisy environment: (a) tracking responses in the buck mode with applied noise of 0.01 variance, (b) tracking responses in the boost mode with applied noise of 0.9 variance



**FIGURE 18** The performance of the controllers feed to different loads: (a) converging operation in resistive–inductive load for buck mode ( $L = 1\mu\text{H}$ ,  $R = 50\Omega$ ), (b) converging operation in resistive–capacitive load for buck mode ( $C = 1\mu\text{F}$ ,  $R = 50\Omega$ ), (c) converging operation in resistive–inductive load for boost mode ( $L = 1\mu\text{H}$ ,  $R = 50\Omega$ ), (d) converging operation in resistive–capacitive load for boost mode ( $C = 1\mu\text{F}$ ,  $R = 50\Omega$ )

Next, to show the tracking operation of the controllers in reference voltage alterations, some positive and negative variations are applied during the working operation of the converter in Figure 15. The first variation belongs to a negative reference signal change of 40–15 V and then a positive rise took place in 15–50 V and finally a negative step is tested for 50–25 V which can



**FIGURE 19** Topology of the buck–boost converter in experimental environment

be a large variation for both of the controllers. A detailed comparison is demonstrated based on Figure 15 in Table 6, which reaffirms a considerable robustness of the adaptive cascade controller in compensating these sudden changes; however, the single loop control method has an approximate tracking with large ripples that is not suitable in industrial applications.

In industrial applications the impact of noise is an inevitable phenomenon that can have the most harmful influence on control procedure. Thus, to stimulate the effect of this disturbance on the system, noise is injected to the system with two levels of 0.01 and 0.1 variances in Figure 16.

The noise applied in Figure 16 in both working modes can cause problems for the controllers. As is obvious from Figure 16, two other designed control strategies face deviations in tracking responses but the adaptive cascade controller shows a remarkable performance in compensating the impact of noise which can present it as a suitable alternative for practical applications.

As mentioned before SLCs are not robust enough in supply voltage variations. To check the performance of the controllers against supply voltage variations, the output voltage is fixed at 30 V and the supply voltage is changed for different levels in Figure 17.

It is clear from Figure 17 that the cascade controller performs really well in various supply voltage alterations; however, a SLC is unable to operate properly. On the other hand, this structure can be changed for different consumers such as a DC motor which is modelled as a resistive–inductive load; hence, the performance of the controllers are tested in two types of load in both of the working modes.

The results driven in Figure 18 totally show that the cascade controller has excellent operation in different loads despite the fact that a change in the load can dramatically influence the dynamics of the system that can cause malfunction of the controller. It should be noted that having an online parametric

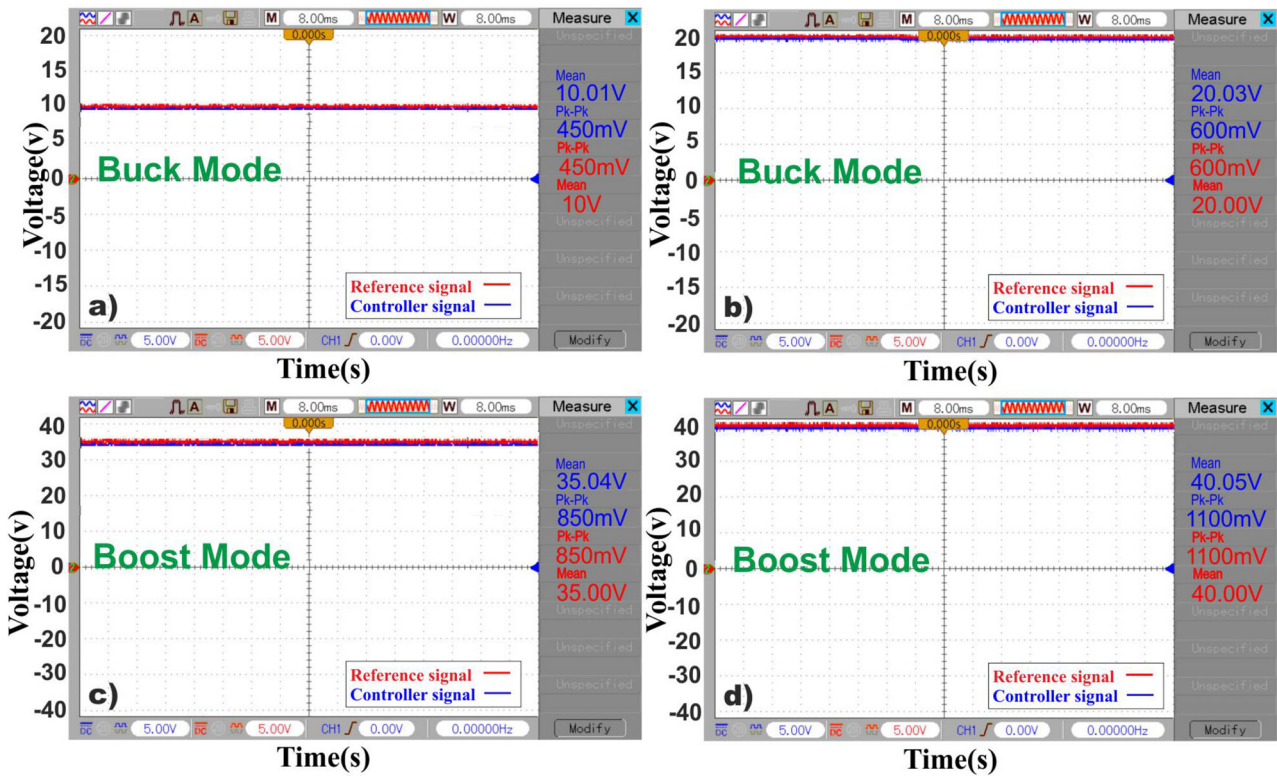


FIGURE 20 Cascade controller on buck–boost converter; (a) tracking response of the controller in buck mode for 10 V, (b) tracking response of the controller in buck mode for 20 V, (c) tracking response of the controller in boost mode for 35 V, (d) tracking response of the controller in boost mode for 40 V

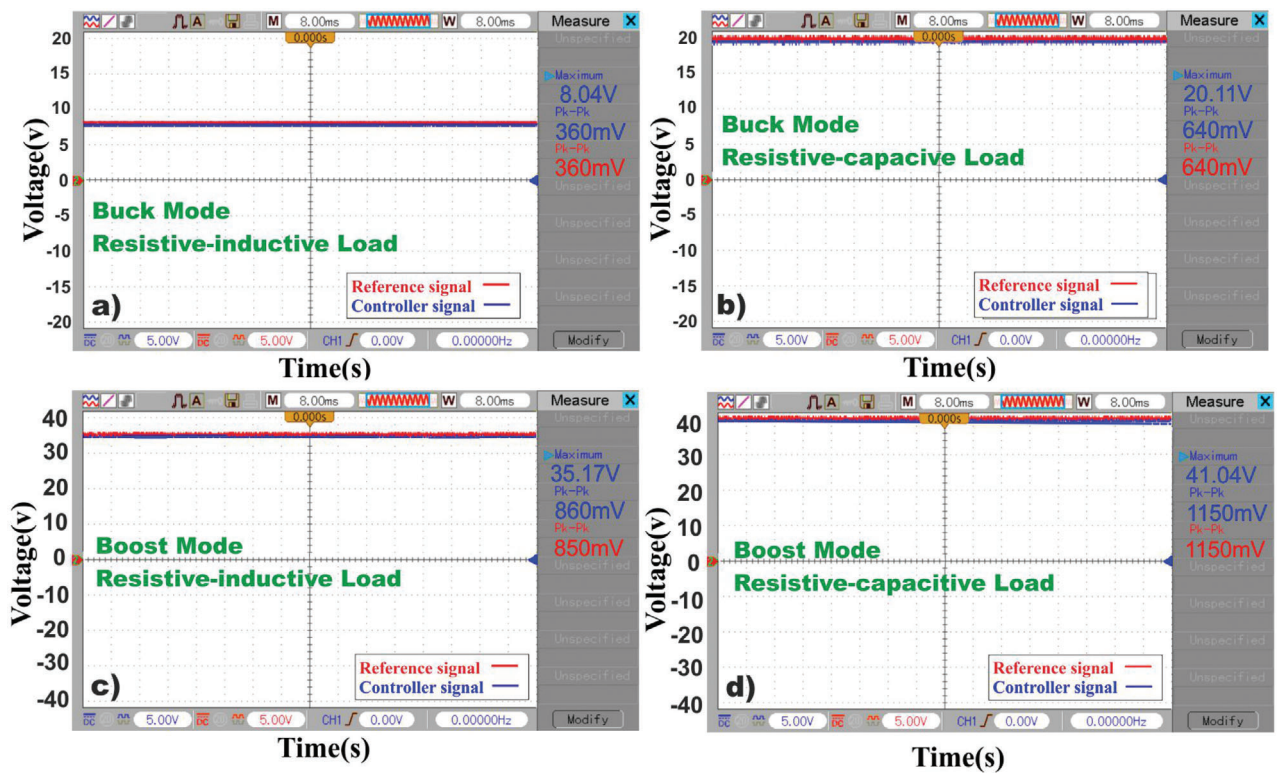
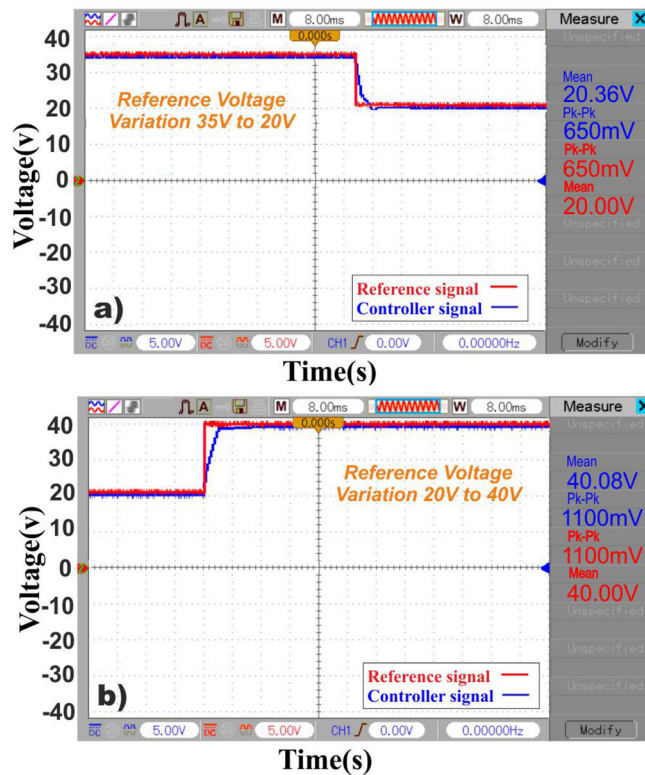


FIGURE 21 Performance of the adaptive cascade controller feed to different loads: (a) converging operation in resistive–inductive load for buck mode ( $L = 1\mu\text{H}$ ,  $R = 30\Omega$ ), (b) converging operation in resistive–capacitive load for buck mode ( $C = 10\mu\text{F}$ ,  $R = 50\Omega$ ), (c) converging operation in resistive–inductive load for boost mode ( $L = 1\mu\text{H}$ ,  $R = 30\Omega$ ), (d) converging operation in resistive–capacitive load for boost mode ( $C = 10\mu\text{F}$ ,  $R = 50\Omega$ )



**FIGURE 22** Operation of the adaptive cascade controller on buck–boost converter in reference signal variations; (a) the convergence in a negative reference voltage change, (b) the convergence in a positive reference voltage change

optimization over the control loops can be a positive aspect in the load variations.

## 8 | EXPERIMENTAL RESULT

ZOH technique is used to discretize the controller. We classify three stages for applying the controlling strategy on the converter; (1) collecting data from the designing software, (2) coding this data to C language and (3) sending the driven code into the digital signal controllers. The PWM technique is utilized to generate a firing signal for a buck–boost converter switches, while in this technique, a square wave signal is sent to the switches produced by a comparison driven between a triangle wave and controller signal. In Figure 19a, hardware real-time implementation of buck–boost converter is demonstrated including power and control structures of the converter, simultaneously.

The prototype machine of Figure 19 is built to elaborate on the accuracy of the presented adaptive cascade control for the converter. As can be seen, different parts and tools are used in this structure as follows: an Arduino processor is working as the core of this topology to convert and generate control signal while the adopted model is UNO-SMD CH340 type, a DC–DC buck–boost converter is built to feed different types of loads including a voltage sensor (LV25-P) and a current sen-

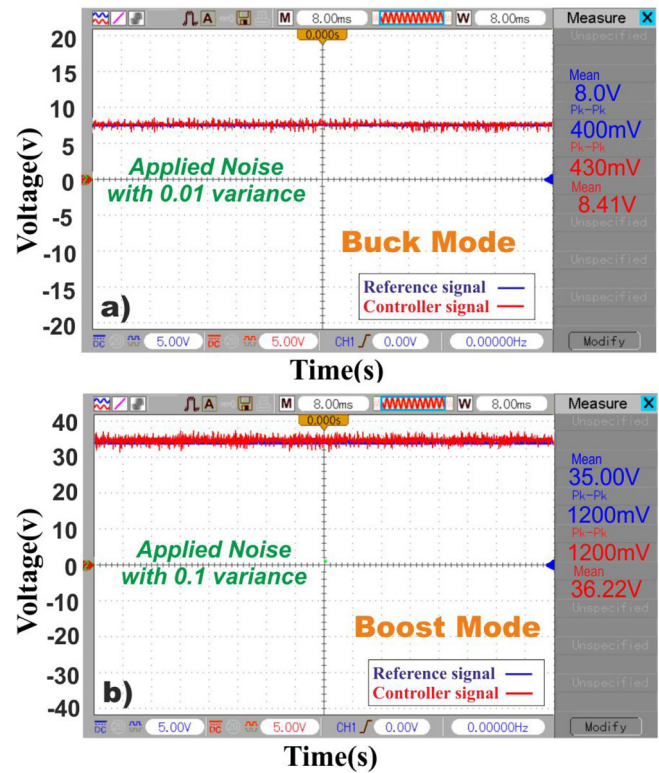


**FIGURE 23** Convergence of the adaptive cascade control method on the buck–boost converter under the impact of noise: (a) controller tracking operation in buck mode with 0.01 variance noise, (b) controller tracking operation in boost mode with 0.1 variance noise

sor (CSNE151-100) to establish the cascade controller, switching components are UF4007 and IRF9630. Furthermore, to decrease computational difficulties of high sampling frequency in the processor, the range of 10 to 20 kHz is selected for switching frequency. A DUE processor converts the voltage and current measured by sensors through its analog-to-digital converter and then generated average values will be uploaded to control loops as inputs. We considered 30 V as the supply voltage of the converter and the aim is to track a voltage of 5 to 50 V on the load using the adaptive cascade controller. Experimental results are acquired in two different modes of the converter in Figures 20–23.

The following experimental results are achieved based on the converter's performance utilizing the adaptive cascade technique with and without considering disturbances. Figure 20 shows the converging operation of the adaptive cascade controller for the references of 10, 20, 30 and 35 V without considering disturbances fed to a resistance ( $R = 10\Omega$ ) which states a significant tracking without containing harmful error.

Since converters are used in practical applications in real-time environments, they encounter various and disturbing factors in their performance. As a result, the proposed controller is examined in real-time situations to verify the performance of the proposed controller. On the other hand, the load fed to the converter in Figure 20 is a pure resistance load which can be changed due to the need of a consumer and depicts a different structure. To test the converter connected to different

load types, two types of load, resistive–capacitive and resistive–inductive, are analysed in both modes by Figure 21.

Changing the load structure feed to the converter can vary the dynamics of a system resulting in difficulties for control procedure. However, observing Figure 21, this presented control scheme is robust enough to compensate for the dynamical differences caused by load changes without a need to be redesigned. In Figure 15, simulation results have been carried out for testing the response of controllers in reference signal changes. Besides, to drive this experiment in real-time condition, two variations are applied on the system in Figure 22. Also, Figure 22 illustrates supply voltage variations in two rising and falling levels. It can be seen that these alternations cannot cause a serious difficulty for the controller and tracking performance is conducted successfully.

Furthermore, the impact of noise is tested on two levels in real-time environment (Figure 23). An excellent robustness is seen for the proposed controller in Figure 23 which can compensate for the negative impact of noise with different rate of variances.

All the results once again reaffirm the great robustness of the adaptive cascaded controller in different working conditions.

## 9 | CONCLUSIONS


Here, an adaptive cascade control scheme is presented by an outer-voltage control loop consist of a FO-PID controller tuned by an ALO algorithm and an inner-current control loop with a self-tuning regulator adaptive controller with a novel IERLS identification method on a buck–boost DC–DC converter. This discussed approach is able to keep the stability margin in a desired limit despite the parametric variations and large signal transients on the DC–DC converter. Moreover, the adaptive cascade controller used a novel optimization algorithm in the outer loop which is able to tune the gains of FO-PID with better values; however, a novel identification algorithm is introduced for the inner loop showing better parametric estimations in challenging conditions with faster dynamic in comparison with the outer loop. The proposed control method provided better convergence to the reference signal in comparison with a single loop PSO based PID controller in different working situations. Both experimental and simulation results reaffirm noticeable improvements in the performance of the converter in both operating modes when considering harmful disturbances.

## CONFLICT OF INTEREST

The authors declare no conflict of interest.

## ORCID

Hasan Mollaei  <https://orcid.org/0000-0002-3859-994X>

Seyyed Morteza Ghamari  <https://orcid.org/0000-0001-5082-820X>

Seyyed Amirhossein Saadat  <https://orcid.org/0000-0001-6101-9934>

Patrick Wheeler  <https://orcid.org/0000-0003-2509-9767>

## REFERENCES

- Jung, M., et al.: Perovskite precursor solution chemistry: from fundamentals to photovoltaic applications. *Chem. Soc. Rev.* 48(7), 2011–2038 (2019)
- Bacha, S., Munteanu, I., Bratcu, A.I.: Power electronic converters modeling and control. *Advanced Textbooks in Control and Signal Process.* 454, 454 (2014)
- Priyadarshi, N., et al.: An experimental study on zeta buck–boost converter for application in PV system. *Handbook of Distributed Generation*, pp. 46, 6 393–406. Springer, Cham (2017)
- Kaouane, M., Boukhelifa, A., Cheriti, A.: Regulated output voltage double switch Buck-Boost converter for photovoltaic energy application. *Int. J. Hydrogen Energy* 41(45), 20847–20857 (2016)
- Zhang, G., et al.: Advanced four-mode-modulation-based four-switch non-inverting buck–boost converter with extra operation zone. *IET Power Electron.* 13(10), 2049–2059 (2020)
- González-Castaño, C., et al.: Coupled inductors design of the bidirectional non-inverting buck–boost converter for high-voltage applications. *IET Power Electron.* 13(14), 3188–3198 (2020)
- Fishelov, A., Gazit, M., Radimov, N.: Digital average input current control in power converter. *U.S. Patent* 10(116), 217, issued October 30, 2018
- Lu, Y., Ki, W.-H., Yue, C.P.: An NMOS-LDO regulated switched-capacitor DC–DC converter with fast-response adaptive-phase digital control. *IEEE Trans. Power Electron.* 31(2), 1294–1303 (2015)
- Fei, J., Chen, Y.: Dynamic terminal sliding-mode control for single-phase active power filter using new feedback recurrent neural network. *IEEE Trans. Power Electron.* 35(9), 9906–9924 (2020)
- Babaie, M., et al.: Switching-based optimized sliding-mode control for capacitor self-voltage balancing operation of seven-level PUC inverter. *IEEE Trans. Ind. Electron.* 68(4), 3044–3057 (2020)
- Rasool, M. A. U., Khan, M. M., Faiz, M. T., Tahir, S., & Zhang, W. (2018, September). An Optimized Disturbance Observer Based Digital Deadbeat Control Technique for Three-Phase Voltage Source Inverter. In *Proceedings of the 2018 International Conference on Electronics and Electrical Engineering Technology* (pp. 27–33).
- Pichan, M., Rastegar, H., Monfared, M.: Deadbeat control of the stand-alone four-leg inverter considering the effect of the neutral line inductor. *IEEE Trans. Ind. Electron.* 64, (4), 2592–2601 (2016)
- Li, X., Liu, Y., Xue, Y.: Four-Switch Buck-Boost Converter Based on Model Predictive Control with Smooth Mode Transition Capability. *IEEE Trans. Ind. Electron.* (2020)
- Malathi, S., Elango, K.: Implementation of dead beat controller using Particle Swarm Optimization for software defined network. *Comput. Commun.* 155, 235–243 (2020)
- Restrepo, Carlos, et al.: "Current control of the coupled-inductor buck–boost DC–DC switching converter using a model predictive control approach." *IEEE Journal of Emerging and Selected Topics in Power Electronics* 8.4 (2020): 3348–3360.
- Zhang, X., et al.: Deadbeat control for single-inductor multiple-output DC–DC converter with effectively reduced cross regulation. *IEEE Journal of Emerging and Selected Topics in Power Electronics* 8(4), 3372–3381 (2019)
- Malekzadeh, M., Khosravi, A., Tavan, M.: A novel adaptive output feedback control for DC–DC boost converter using immersion and invariance observer. *Evolving Systems* 11(4), 707–715 (2020)
- Wu, J., Lu, Y.: Adaptive backstepping sliding mode control for boost converter with constant power load. *IEEE Access* 7(13), 50797–50807 (2019)
- Naik, K.A., Gupta, C.P., Fernandez, E.: Design and implementation of interval type-2 fuzzy logic-PI based adaptive controller for DFIG based wind energy system. *International Journal of Electrical Power & Energy Syst.* 115, 105–128 (2020)
- Mohamed, A.A., et al.: Predictive neural network based adaptive controller for grid-connected PV systems supplying pulse-load. *Sol. Energy* 193, 139–147 (2019)
- Basaran, K., Cetin, N.S.: Designing of a fuzzy controller for grid connected photovoltaic system's converter and comparing with PI controller. In: 2016 IEEE International Conference on Renewable Energy Research and Applications (ICRERA). IEEE, New York (2016)



22. Nouri, A., et al.: DSP-based implementation of a self-tuning fuzzy controller for three-level boost converter. *Electr. Power Syst. Res.* 146(87), 286–297 (2017)
23. Ghamari, S.M., Mollae, H., Khavari, F.: Robust self-tuning regressive adaptive controller design for a DC–DC BUCK converter. *Measurement* 174, 109071 (2021)
24. Ghamari, S.M., Mollae, H., Khavari, F.: Design of robust self-tuning regulator adaptive controller on single-phase full-bridge inverter. *IET Power Electron.* 13(16), 3613–3626 (2020)
25. Fang, W., Liu, X. D., Liu, S. C., & Liu, Y. F. (2014). A digital parallel current-mode control algorithm for DC–DC converters. *IEEE Transactions on Industrial Informatics*, 10(4), 2146–2153.
26. Suryanarayana, K., et al.: Analysis and modeling of digital peak current mode control. In 2012 IEEE International Conference on Power Electronics, Drives and Energy Systems (PEDES) (pp. 1–6). IEEE (2012, December)
27. Grote, T., et al.: Adaptive Digital Slope Compensation for Peak Current Mode Control. 76, 6 3523–3529. University of Paderborn, Paderborn (2009)
28. Biswal, M.: Control Techniques of DC–DC Buck Converter with Improved Performance. 7, 2 1–430. National Institute of Technology, Rourkela (2011)
29. Kularatna: Electronic circuit design: from concept to implementation. Published September 19, 2019 by CRC Press 502 Pages (2019)
30. Kazi, M.A., et al.: Minimization of Transients in Buck Converter Using Cascade Control Techniques. *Eng. Sci. Technol. International research Journal-ESTIRJ* 1(4), 1–8 (2017)
31. Bellinaso, L.V., et al.: Cascade control with adaptive voltage controller applied to photovoltaic boost converters. *IEEE Trans. Ind. Appl.* 55(2), 1903–1912 (2018)
32. Remes, C.L., et al.: LQG controller in cascade loop tuned by PSO applied to a DC–DC converter. *Asian J. Control* (2020)
33. Kim, E.S., Kim, C.J., Kim, Y.T.: Cascade Controller Design for Cuk Converter. In 2018 21st International Conference on Electrical Machines and Systems (ICEMS) (pp. 2423–2426). IEEE (2018, October)
34. Bellinaso, L.V., et al.: Cascade control with adaptive voltage controller applied to photovoltaic boost converters. *IEEE Trans. Ind. Appl.* 55(2), 1903–1912 (2018)
35. Komathi, C., Umamaheswari, M.G.: Analysis and design of genetic algorithm-based cascade control strategy for improving the dynamic performance of interleaved DC–DC SEPIC PFC converter. *Neural Comput. Applic.* 32(4), 5033–5047 (2019)
36. Ahmad, F., et al.: A robust cascaded controller for DC-DC Boost and CUK converters. *World J. Eng.* (2017)
37. Hidalgo-Reyes, J.I., et al.: Classical and fractional-order modeling of equivalent electrical circuits for supercapacitors and batteries, energy management strategies for hybrid systems and methods for the state of charge estimation: A state of the art review. *Microelectron. J.* 85, 109–128 (2019)
38. Tarasov, V.E.: Review of some promising fractional physical models. *Int. J. Mod. Phys. B* 27, 1330005(27), 1004–1019 (2013)
39. Vinagre, B., Feliu, V.: Modeling and control of dynamic system using fractional calculus: Application to electrochemical processes and flexible structures. In: Proceedings of the 41st IEEE Conference on Decision and Control, pp. 214–239 (2002)
40. Erickson, R., Marsimovic, D.: *Fundamentals of Power Electronics*, Kluwer Academic Publishers, Norwell, MA (2001)
41. Kumar, L., Jain, S.: Multiple-input DC/DC converter topology for hybrid energy system. *IET Power Electron.* 6(8), 1483–1501 (2013)
42. Muñoz-Vázquez, A.J., et al.: Adaptive robust control of fractional-order systems with matched and mismatched disturbances. *Math. Comput. Simul.* 162, 85–96 (2019)
43. Arthi, G., Park, J., Suganya, K.: Controllability of fractional order damped dynamical systems with distributed delays. *Math. Comput. Simul.* 165, 74–91 (2019)
44. Mirjalili, S.: The ant lion optimizer. *Adv. Eng. Software* 83(7), 80–98 (2015)
45. Heidari, A.A., et al.: Ant lion optimizer: Theory, literature review, and application in multi-layer perceptron neural networks. *Nature-Inspired Optimizers*, pp. 45, 3 23–46. Springer, Cham (2020)
46. Abualigah, L., et al.: Ant lion optimizer: a comprehensive survey of its variants and applications. *Arch. Comput. Methods Eng.* 28(3), 1397–1416 (2021)
47. Li, J., Pan, K., Su, Q.: Sensor fault detection and estimation for switched power electronics systems based on sliding mode observer. *Appl. Math. Comput.* 353(6), 282–294 (2019)
48. de Jesús Rubio, J.: SOFMLS: Online self-organizing fuzzy modified least-squares network. *IEEE Trans. Fuzzy Syst.* 17(6), 1296–1309 (2009)
49. Guo, L., Hung, J.Y., Mark Nelms, R.: Evaluation of DSP-based PID and fuzzy controllers for DC–DC converters. *IEEE Trans. Ind. Electron.* 56(6), 2237–2248 (2009)
50. Ghamari, S.M., Gholizadeh-Narm, H., Khavari, F.: Robust adaptive controller design for DC-DC SEPIC converter in photo voltaic application. In 2019 6th International Conference on Control, Instrumentation and Automation (ICCIA), pp. 1–6. IEEE, (2019)
51. Åström, K.J., Björn, W. Adaptive control. Courier Corporation, Addison-Wesley; Subsequent edition (December 1, 2013), 574 pages (2013)
52. Ogata, K.: *Modern control engineering*. Instructor 201709, Pearson; 5th edition (August 25, 2009), 912 pages (2017)

**How to cite this article:** Mollae, H., et al.: A novel adaptive cascade controller design on a buck–boost DC–DC converter with a fractional-order PID voltage controller and a self-tuning regulator adaptive current controller. *IET Power Electron.* 14, 1920–1935 (2021). <https://doi.org/10.1049/pel2.12159>